

## Investigation of vertical velocity distribution in debris flows by PIV measurement

Huayong Chen, Kaiheng Hu, Peng Cui & Xiaoqing Chen

To cite this article: Huayong Chen, Kaiheng Hu, Peng Cui & Xiaoqing Chen (2017) Investigation of vertical velocity distribution in debris flows by PIV measurement, Geomatics, Natural Hazards and Risk, 8:2, 1631-1642, DOI: [10.1080/19475705.2017.1366955](https://doi.org/10.1080/19475705.2017.1366955)

To link to this article: <https://doi.org/10.1080/19475705.2017.1366955>



© 2017 The Author(s). Published by Informa UK Limited, trading as Taylor & Francis Group



Published online: 31 Aug 2017.



Submit your article to this journal [↗](#)



Article views: 1095



View related articles [↗](#)







View Crossmark data [↗](#)



Citing articles: 3 View citing articles [↗](#)



# Investigation of vertical velocity distribution in debris flows by PIV measurement

Huayong Chen <sup>a,b</sup>, Kaiheng Hu <sup>a,b</sup>, Peng Cui <sup>a,b,c</sup> and Xiaoqing Chen <sup>a,b,c</sup>

<sup>a</sup>Key Laboratory of Mountain Hazards and Earth Surface Process, Institute of Mountain Hazards and Environment, Chinese Academy of Sciences (CAS), Chengdu, Sichuan, China; <sup>b</sup>University of Chinese Academy of Sciences, Beijing, China; <sup>c</sup>CAS Center for Excellence in Tibetan Plateau Earth Sciences, Beijing, China

## ABSTRACT

Vertical velocity distribution in some fluid–solid flows such as debris flows has not been well recognized and lacked a commonly accepted form. The particle image velocimetry (PIV) measurement system was employed to investigate the velocity distribution of high-viscosity fluid–solid flows. The velocity distribution was greatly affected by the particles due to the particle–particle collision and momentum exchange between the particle and fluid. Both of them show a similar increasing trend only in the range of the dimensionless flow depth from 0 to 0.7. In addition, based on the log-law model for sediment-laden flows, a modified model was proposed to predict vertical velocity distribution in debris flows. The results indicated that the calculated results were in good agreement with the experimental ones. The coefficient and index for the modified item was about 0.92 and  $-1/6$ , respectively.

## ARTICLE HISTORY

Received 1 March 2017

Accepted 7 August 2017

## KEYWORDS

Vertical velocity distribution; debris flow; particle image velocimetry (PIV); flow viscosity; log-law model

## 1. Introduction

Debris-flow velocity distribution form is one of the most complex problems in the dynamic mechanism of this kind of solid-fluid mixture flow due to the flow's opacity caused by its high concentration of solid particles (Han et al. 2014). In order to better understand the behavior of debris flows, different measurement methods were employed to obtain debris flow velocity. The measurement devices such as ultrasonic sensors, radar, or seismic sensors were introduced to monitor the debris-flow velocity (Arattano 2003; Hürlimann 2003; Mc Ardell et al. 2003; Arattano and Marchi 2005; Prochaska et al. 2008; Wei et al. 2012). Some other empirical equations have also been proposed to estimate the debris flow velocity based on Manning formula (Fei et al. 2002; Tang et al. 2011; Cui et al. 2013). Numerical simulation methods were employed to investigate velocity of the flow fronts, sediment entrainment from the erodible bed, transportation process based on the depth-averaged motion equations (Joo de and van Steijn 2003; Mangeney et al. 2007; Armanini et al. 2009; Hungr and McDougall 2009; Luna et al. 2012; Han et al. 2015; Han et al. 2016; Wang et al. 2016). The debris flow velocity mentioned above was an instantaneous velocity at flow front or an average velocity over a certain distance. In some literatures, the impact forces at different flow depths were obtained by the impact force sensors to investigate internal velocity distribution along flow depth in an indirect way (Yang et al. 2011).

Although the mean velocity of debris flows was obtained by analyzing the dynamic process, information on the particle or fluid velocity distribution through the flow depth or fluctuating

velocity in debris flows was rather rare. Along with the development of computing power and image-processing techniques, particle image velocimetry (PIV) becomes a popular technique in two phase flows due to its non-invasive measurement, full-field, instantaneous flow velocity maps, especially, in solid-water mixtures. PIV was applied to measure both fluid and particulate phase simultaneously and turbulence intensities were calculated (Liu and Lam 2014). The characteristics of liquid-phase, such as mean velocities, turbulent kinetic energy, and energy dissipation, were analyzed in detail when the particles were seeded at different particle concentrations (Unadkat et al. 2009; Gabriele et al. 2011). The effects of particle concentration (1%–9% by volume) and diameter (1–2 mm) on axial liquid velocities and turbulence were investigated. The results indicated that mean axial velocities in the impeller region decreased by up to 50% with increasing solids content. The magnitude of turbulence enhancement increased with both particle size and concentration (Virdung and Rasmuson 2007). These experimental studies focused on the dynamic characteristics of continuous phase with very low viscosity, but rarely on the characteristics of the flows with both relatively high viscosity and particles simultaneously. A new PIV software was developed to capture the particular features of the flows in GITS-UPC channels and to obtain velocity profiles (Medina and Bateman 2010).

In this study, the mixture of two different transparent liquids (Machine oil and white oil) that has similarly high viscosity with diluted debris flows was used to substitute the fluid phase of the debris flows in flume experiments. PIV was employed to measure instantaneous velocity field. The velocity distribution through the flow depth was analyzed based on the experimental results. In addition, the modified theoretical model was proposed to predict the vertical velocity distribution of debris flows based on the log-law model for sediment-laden flow.

## 2. Design of simulated experiments

### 2.1. Experimental setup

The experimental setup consisted of a tank, a sluice gate, a rectangular flume, and a tailing pool (Figure 1). The rectangular channel was about 4.5 m long, 0.2 m wide and 0.4 m high, with adjustable channel slope angles ranging from  $4^\circ$  to  $10^\circ$ . For the solid-liquid flow, a mixed viscous liquid with a density of  $0.91 \text{ kg/cm}^3$  is chosen as the liquid phase, and the spherical glass beads with a density of  $2.48 \text{ g/cm}^3$  are used as the solid phase. In a static condition, the spherical glass bead falls to the bottom due to its higher density compared to the liquid. In order to simulate debris flows (fully mixed between solid and liquid phase), the mixed viscous liquid was held in the tank (upstream) and the spherical glass beads was set 1.0 m away from the sluice gate (downstream). In each experimental run, a certain volume of the viscous liquid was firstly put into the tank, and then a layer of spherical glass beads with uniform diameter (0.2 m in length and 0.01 m in thickness) was set on the bottom of the channel as shown in Figure 1. When the sluice gate was lifted up the viscous liquid ran down due to gravity. When the accelerated viscous liquid passed the spherical glass beads, the beads were entrained and transported with the viscous flow. Two particle sizes for the uniform spherical glass

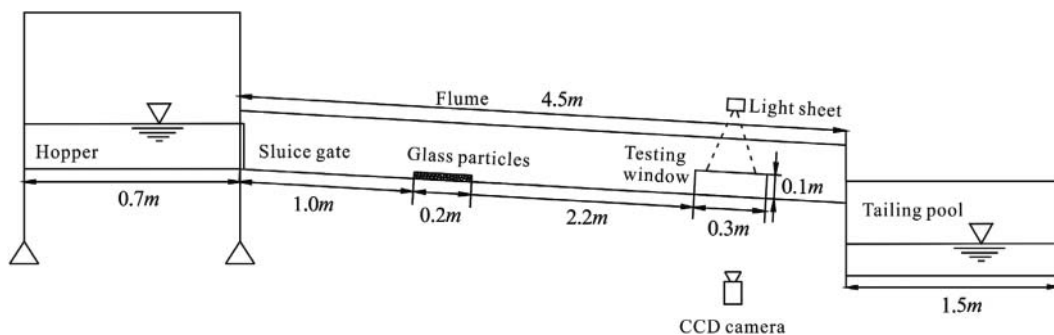


Figure 1. Schematic diagram of the experimental setup.

**Table 1.** The detailed hydraulic parameters for the experiments.

Run number	$D$ (mm)	$S$ (°)	$M$ (kg)	$h$ (mm)	$U$ (m/s)	$R$ (m)	$Fr$
1	0.50	4.00	10.00	12.61	0.83	0.01	2.36
2	0.50	4.00	15.00	16.81	0.79	0.01	1.95
3	0.50	4.00	20.00	23.99	0.85	0.02	1.75
4	0.50	4.00	25.00	29.52	0.82	0.02	1.52
5	0.50	7.00	10.00	15.19	1.17	0.01	3.03
6	0.50	7.00	15.00	15.59	1.09	0.01	2.79
7	0.50	7.00	20.00	19.63	1.26	0.02	2.87
8	0.50	7.00	25.00	22.29	1.23	0.02	2.63
9	0.50	10.00	10.00	13.11	1.33	0.01	3.71
10	0.50	10.00	15.00	16.67	1.15	0.01	2.85
11	0.50	10.00	20.00	23.53	1.35	0.02	2.81
12	0.50	10.00	25.00	25.26	1.40	0.02	2.81
13	1.00	4.00	10.00	12.44	0.71	0.01	2.03
14	1.00	4.00	15.00	18.43	1.00	0.02	2.35
15	1.00	4.00	20.00	24.11	0.73	0.02	1.50
16	1.00	4.00	25.00	29.42	0.92	0.02	1.71
17	1.00	7.00	10.00	16.26	1.15	0.01	2.88
18	1.00	7.00	15.00	17.16	1.06	0.01	2.58
19	1.00	7.00	20.00	19.75	1.08	0.02	2.45
20	1.00	7.00	25.00	23.20	1.16	0.02	2.43
21	1.00	10.00	10.00	14.18	1.20	0.01	3.22
22	1.00	10.00	15.00	16.62	1.20	0.01	2.97
23	1.00	10.00	20.00	24.31	1.23	0.02	2.52
24	1.00	10.00	25.00	27.76	1.37	0.02	2.63

beads, four liquid scale, and three channel slopes were considered in present work. The detailed hydraulic parameters for each run were shown in Table 1.

## 2.2. Fundamental principle of the PIV measurement

PIV measurement system mainly consisted of the laser, the optics, a CCD (Charge Coupled Device) camera, a synchronizer, and a computer. The laser was directed through a series of optical components which shaped the beam into a thin planar sheet of laser light (laser knife). The flow with tracers were illuminated by the light sheet and captured by the CCD camera (Nikon 630059 Power view Plus with  $2048 \times 2048$  pixels CCD array size). Different from the spherical glass beads, the tracers are tiny particles with very small diameters ( $10^{-6}$ – $10^{-4}$  m) such as the fluorescent seeding particles, or hollow glass microspheres, which have good following performance. Therefore, they have the similar velocity with that of the liquid. By monitoring the movement of the tracer particles, the velocities of the fluid can be measured accordingly. The computer was employed to control the system and stored the experimental data. The camera and the laser were connected through a synchronizer, which was controlled by a computer and dictated the timing of the camera sequence in conjunction with the firing of the laser. A CCD camera was set by the side to capture the film of debris flows in the PIV system as shown in Figure 2(a) (Di Cristo 2011). In the PIV measurement system, the temporal frame separation between Frame A and Frame B was 100  $\mu$ s, and the size of the interrogation windows for image evaluation is  $64 \times 64$  pixels. Correlation values are calculated by using Fast Fourier Transform (FFT). Data obtained from saturated images are about 90%. The velocity of the tracers can be calculated as (Figure 2(b); Wereley and Meinhardt 2010):

$$\begin{cases} v_x = \frac{\Delta x}{\Delta t} \approx \frac{x_2(t + \Delta t) - x_1(t)}{\Delta t} = \bar{v}_x \\ v_y = \frac{\Delta y}{\Delta t} \approx \frac{y_2(t + \Delta t) - y_1(t)}{\Delta t} = \bar{v}_y \end{cases} \quad (1)$$

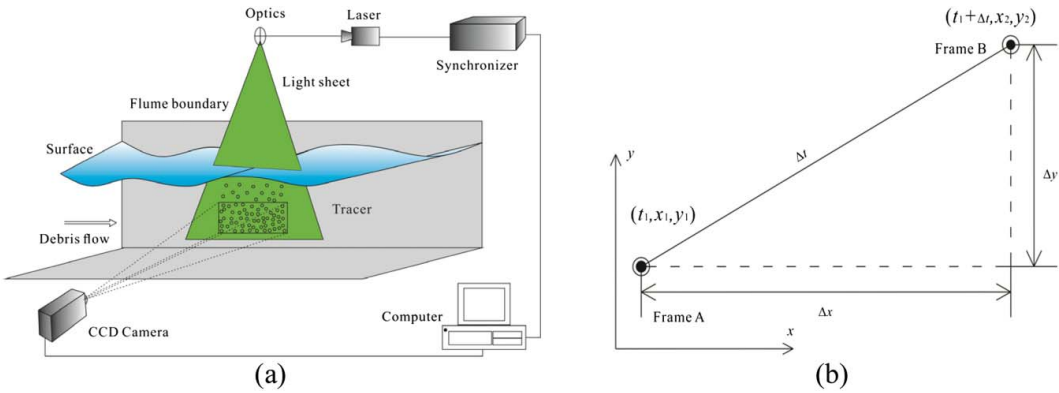


**Figure 2.** Fundamental principle of the PIV measurement: (a) the basic composites of the velocity measurement system; (b) the instantaneous velocity measurement based on two sequential frames.

where  $v_x, v_y$  is the particle velocity in the  $x$  and  $y$  direction, respectively;  $\Delta x$  is the displacement in the  $x$  direction at time interval  $\Delta t$ ;  $\Delta y$  is the displacement in the  $y$  direction at time interval  $\Delta t$ ;  $\bar{v}_x, \bar{v}_y$  is the mean velocity in the  $x$  and  $y$  direction, respectively (Figure 2(b)).

**2.3. Rheological feature of the mixing fluid**

When PIV is employed to measure the profile of debris flow velocity through flow depth the fluid transparency and relative low solid concentration should be considered. For the diluted debris flow, the viscosity may be relative small (Parsons et al. 2001; Iverson 2012), a mixture of two transparent fluid (32# machine oil, 2.0 Pa·s at 25 °C; white oil, 0.001 Pa·s at 25 °C) was used to simulate the diluted debris flow. Variation of the mixture transparent fluid at different ratios was shown in Figure 3. A ratio of 3:1 of Machine oil and white oil was set in the experiment. The viscosity of the mixture fluid was about 0.01 Pa·s which was about ten times as large as that of pure water. The mixture flowed over the erodible bed, forming the two-phase flow with relatively high viscosity. PIV was set at the end of the flume for velocity field measurement when the flow was under the fully developed and steady-state flow condition.

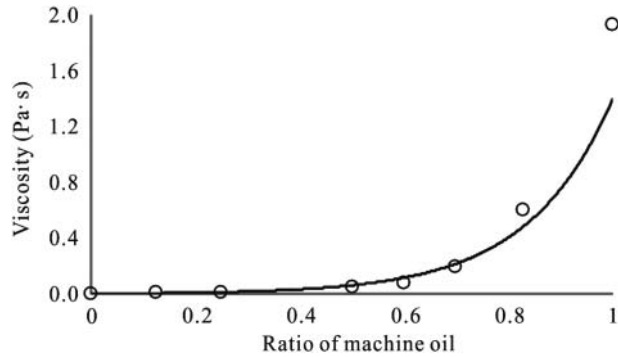


**Figure 3.** Viscosity of the mixture fluid vs. ratio of machine oil.

### 3. Results and discussion

#### 3.1. Typical debris flow patterns

Figure 4 indicated that the vertical distribution of particles in debris flows was different from that in sediment-laden flows. In the latter flows, the most particles usually moved near the flume bottom, only small portion of particles were observed in the upper layer (Figure 4(a,c,e)), while in the former flows we found that the distribution of particles along flow depth was more uniform. The particles not only moved near the flume bottom but also jumped to the upper layer. Difference of the particle distribution was explained by the different fluid viscosity. The particles which were initialized by flow easily fell down to bottom in the sediment flow due to low fluid viscosity. In the debris flows higher fluid viscosity hindered the fast settling of the sediment particles, keeping them moving longer distance along flume before falling back to bottom. Therefore, during a certain period of time more sediment particles were observed to keep moving in the debris flows (Figure 4(b,d,f)).

#### 3.2. Velocity distribution in debris flows

Based on the processing procedure of PIV system, the velocity distribution in the testing window was obtained. In order to avoid the effect of over concentrated (pink color in Figure 4) on the flow field analysis, the 'Local Validation' (which means using the vectors in the neighborhood of each vector to calculate a reference vector for validation) and 'Vector Conditioning' (which is used after vector validation to fill holes in the vector field and/or to smooth the vector field) was employed to modify the flow field in PIV processing. As we know that in clear water, the velocity increases gradually with increasing the flow depth and the maximum velocity appears near the water surface (Guo and Julien 2001; Balachandar and Patel 2005). However, in the debris flows the maximum velocity

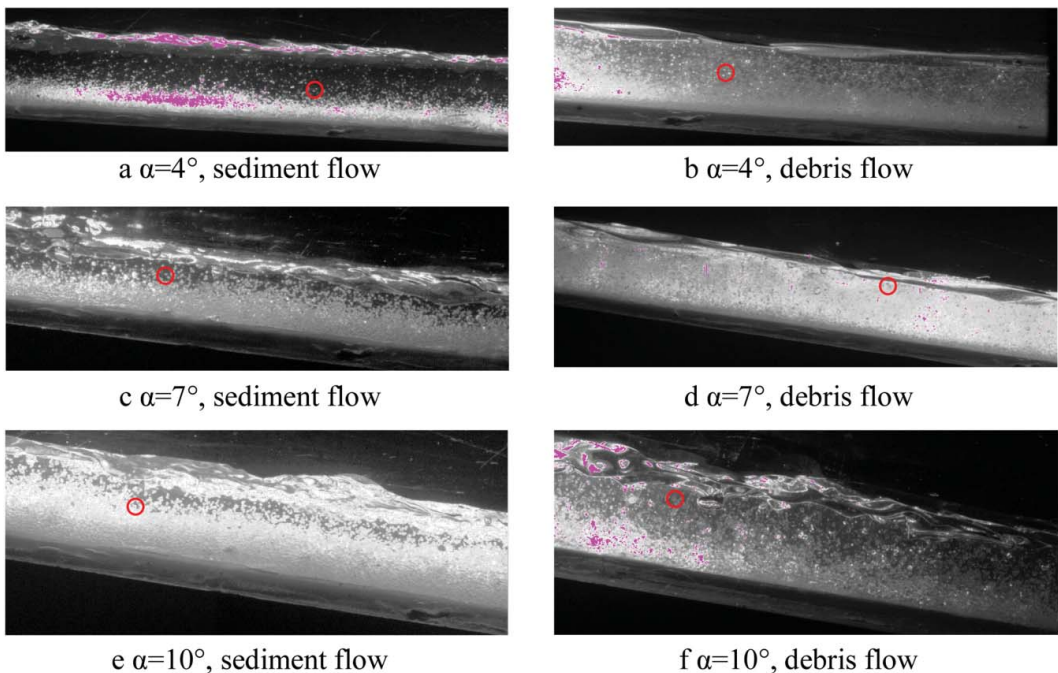


**Figure 4.** Comparison of particle distribution for sediment-laden flows and debris flows: for (a, c, and e), the liquid phase was clear water; for (b, d, and f), the liquid phase was mixture of 32# machine oil and white oil. The spherical glass beads in clear water were easily falling down due to low viscosity and obvious stratification was found in (a, c, and e). However, the spherical glass beads distributed relatively uniformly in (b, d, and f). The spherical glass beads were illuminated by the laser as shown 'gray points' in red circle.



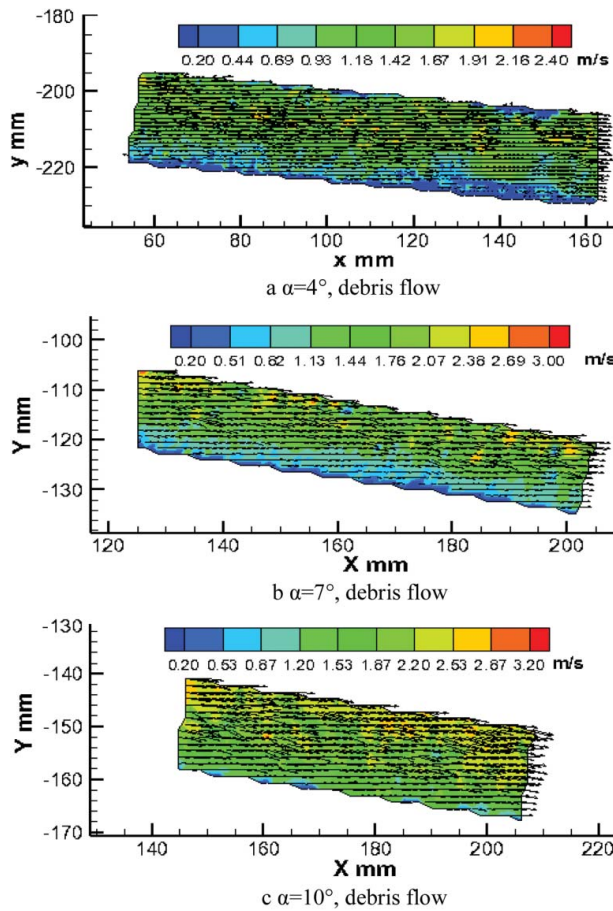


**Figure 5.** The velocity field distribution for debris flow at different channel slopes (the arrows represent absolute mean velocity of the fluid phase).

(shown in red color in Figure 5) didn't always appear near the flow surface in the whole region. In some areas it appeared below the free surface. It was found that the velocity distribution of debris flow was much different from that in clear water. Flow velocity was greatly affected by the particles in debris flows due to the particle-particle collision and momentum exchange between the particle and fluid. The collision changed the particle velocity and the motion of fluid around the particles at the same time. In general, the maximum velocity at  $\alpha = 4^\circ$ ,  $\alpha = 7^\circ$ ,  $\alpha = 10^\circ$ , occurring in the upper layer of the flows, was about 2.4, 3.0, 3.2 m/s, respectively as shown in Figure 5(a–c).

### 3.3. Velocity profile along flow depth at different slope angles

Compared with the traditional point-wise velocimetry, PIV can obtain the whole instantaneous and mean velocity field without disturbing the debris flows. The debris flow velocity profile along flow depth can be analyzed based on the information of the mean velocity field. As shown in Figure 5 we can find that the values of flow velocity at a certain depth is not a constant due to the turbulence and non-uniform distribution of particles in the debris flows. Therefore, we chose three different lines and then calculated the average velocity through flow depth. Figure 6 shows the variation of velocity profile at different slope angles. Although the velocity magnitude was different at different slope angles, the dimensionless debris flow velocity ( $u/u_0$ ,  $u_0$  is maximum velocity through flow depth) followed the similar trend through the flow depth. With increasing debris flow depth, the

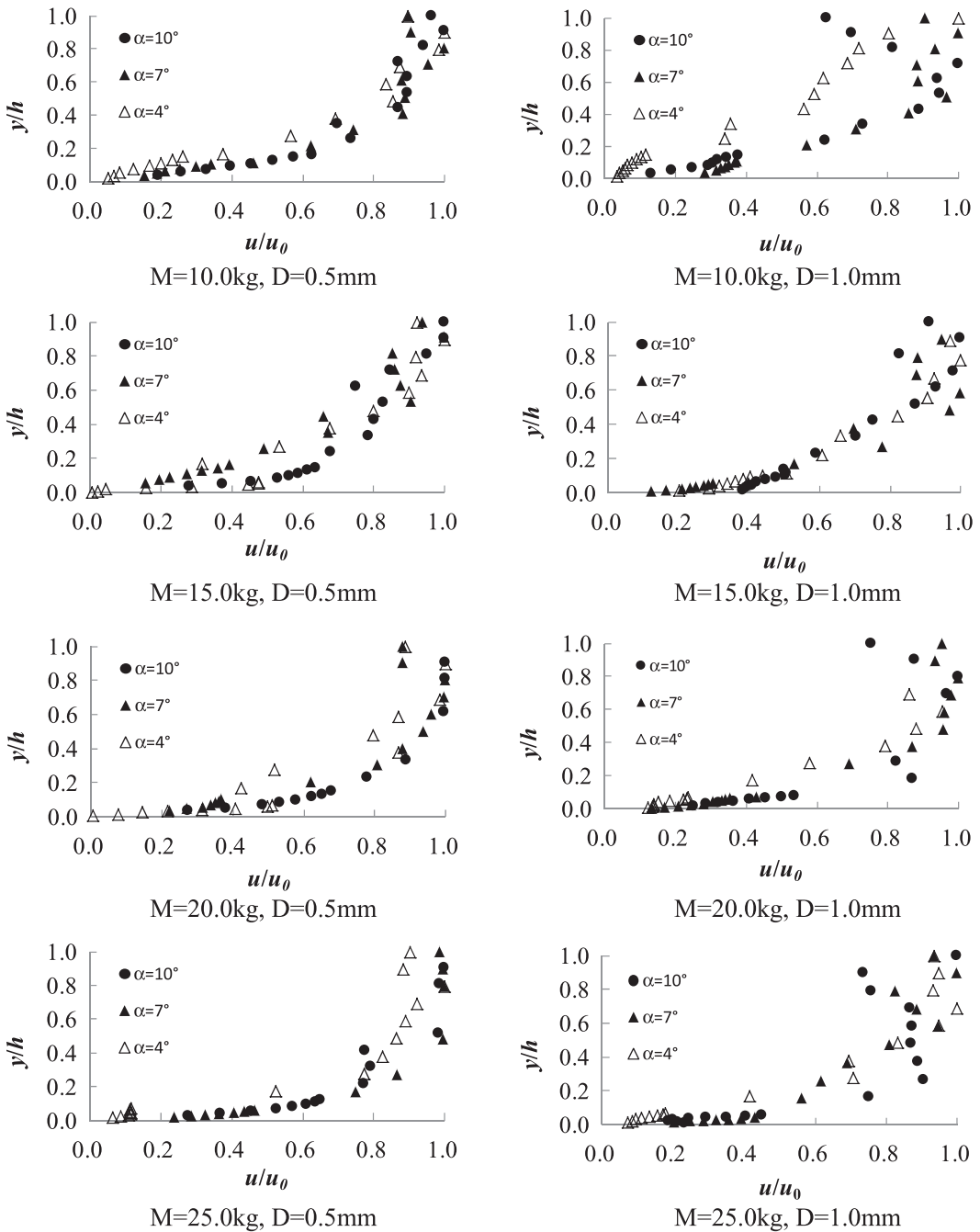


**Figure 6.** Effects of slope angles on velocity profile of debris flow along flow depth.

debris flow velocity increased when dimensionless flow depth ranged from 0 to 0.7. The maximum value in some cases appeared in the upper layer ( $0.7 < y/h < 1.0$ ) but not always appeared at  $y/h = 1.0$  (like the velocity dip phenomenon). The particles with smaller diameter were more easily entrained and transported by debris flows than those with larger diameter. The finer particles had slightly effects on dynamic characteristics of debris flows, correspondingly. So the variation of



vertical velocity at different slopes was in good agreement with each other when  $D = 0.5$  mm. In contrast, it scattered in a relatively wide range when  $D = 1.0$  mm.

### 3.4. Modification of the log-law for velocity profile

The log-law developed from laboratory experiments was widely used to describe the vertical profile of sediment-laden flows in an open channel (Wang et al. 2001):

$$\begin{cases} \frac{u}{u_*} = \frac{1}{k} \ln \frac{y}{K_s} + B_f \\ \text{Re}_* = \frac{u_* D}{\nu} > 70 \end{cases} \quad (2)$$

where  $u$  is the mean velocity at the cross-section,  $u_*$  is the friction velocity,  $k$  is the von Karman constant  $k = 0.4$ ,  $y$  is the vertical distance from the flume bed,  $K_s$  is hydraulic roughness, the integration constant  $B_f$  is a function of  $K_s$ ,  $D$  is the particle diameter,  $g$  is acceleration of gravity, and  $R$  is hydraulic radius. According the experimental conditions, the value of  $\text{Re}_*$  in each experimental run was larger than 70.

Assuming that maximum velocity also satisfies Equation (2), it can be expressed as follows:

$$\begin{cases} \frac{u_{\max}}{u_*} = \frac{1}{k} \ln \frac{H}{K_s} + B_f \\ \text{Re}_* > 70 \end{cases} \quad (3)$$

Subtracting Equation (2) from Equation (3), then we have

$$\frac{u_{\max} - u}{u_*} = \frac{1}{k} \ln \frac{H}{y}. \quad (4)$$

Equation (4) is used to predict the vertical velocity profile for sediment-laden flow, which is similar to that of clear water flow with logarithmic velocity formula but different von Karman constant  $k$  (Wang et al. 2001). However, the viscosity and particle concentration in debris flows are much different from those in the sediment-laden flows. An example of the vertical velocity profile was shown in Figure 7. Obviously, the particle-particle collision, friction between particles and flow, and friction between different fluid layers with different velocities dissipated some kinetic energy of debris flows. Meanwhile, the high flow viscosity increased the frictional resistance and also dissipated some

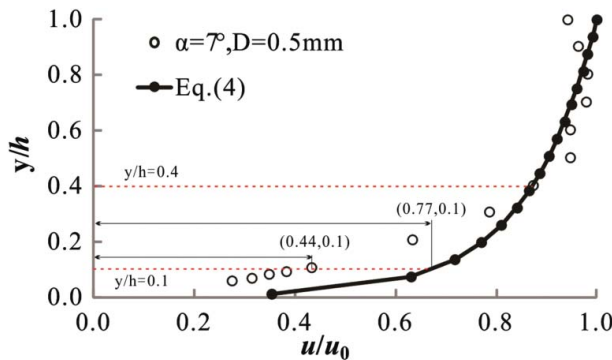


Figure 7. The comparison of theoretical data and experimental ones along flow depth.

kinetic energy during the debris flow motion. Therefore, the velocity at a certain height in debris flow was smaller than that in sediment-laden flows, especially in the lower layer of debris flows ( $y/h < 0.4$ ). It was difficult to obtain the predicted model for debris flow velocity profile by only changing the von Karman constant  $k$ . Additionally, no full understanding of interaction mechanism between the particles and viscous fluid was obtained due to its complexity. It is hardly to quantitate the momentum transfer and energy dissipation at different flow layers. Therefore, no expression has been established to predict the vertical velocity distribution in debris flows. In this paper, a coefficient and a dimensionless parameter  $\frac{H}{y}$  were introduced to modify the existing log-law for sediment-laden flows. Although this parameter can not reveal the interior interaction mechanism between the particles and viscous fluid, it can reflect the variation of flow velocity through flow depth.

The predicted model for the vertical velocity distribution of debris flows was rewritten as follows:

$$\frac{u_{\max} - u}{u_*} = A_1 \left( \frac{H}{y} \right)^B \frac{1}{k} \ln \frac{H}{y} \quad (5)$$

where  $A_1$  is the modification coefficient which is related to the flow viscosity,  $\frac{H}{y}$  is the relative flow depth,  $B$  is the index of the dimensionless flow depth. By comparing the calculated data and the experimental ones, an exponential function with minus index was employed to depict the difference between the calculated and experimental results as shown in Figure 8.

The modified velocity distribution equation was written as follows:

$$\frac{u_{\max} - u}{u_*} = 0.92 \left( \frac{H}{y} \right)^{-\frac{1}{6}} \frac{1}{k} \ln \frac{H}{y}. \quad (6)$$

The comparison of results calculated from Equation (4) and the experimental ones was shown in Figure 9. It indicated that the modified model had considered the effects of particle collision, friction and fluid viscosity on velocity distribution. The calculated data were in good agreement with the results obtained under our experimental conditions. Additionally, some previous investigation on velocity profile of debris flows was shown in Figure 9. It also indicated that the modified model well reproduced the vertical velocity distribution in debris flows. In debris flows, few references can be found in the literature regarding the vertical velocity distribution. The authors referred some previous investigation to calibrate the modified velocity profile, however some discrepancy was found between the previous results and our experimental ones due to the different boundary and initial conditions. Fortunately, in the modified model, the dimensionless parameter  $(H/y)$  can minimize

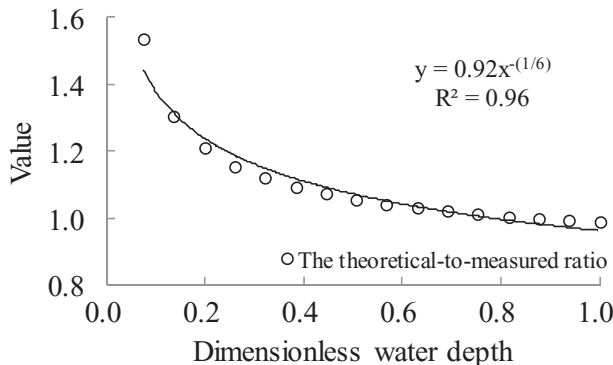


Figure 8. The ration of theoretical data and experimental ones along flow depth.

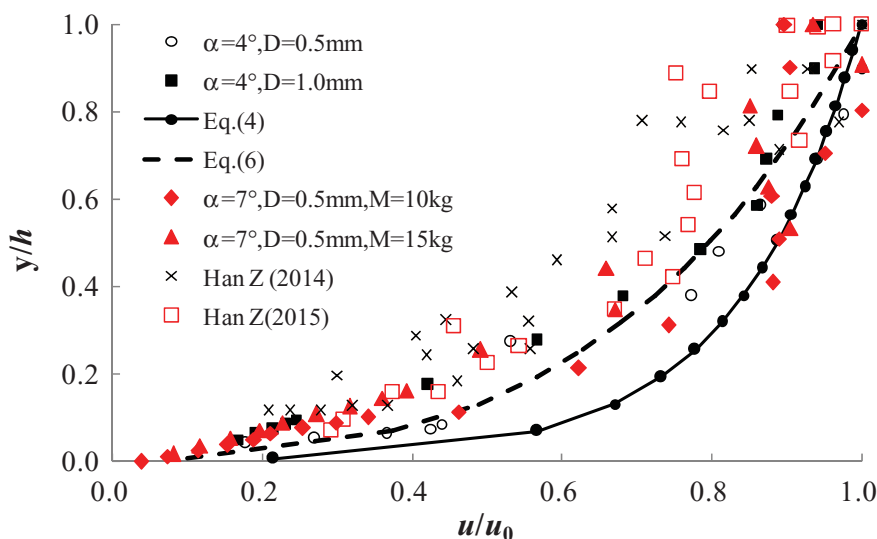


Figure 9. The comparison of calculated data and experimental ones.

the effects of boundary and initial conditions on the results. Therefore, the modified model will have a wide application for vertical velocity distribution prediction in debris flows.

#### 4. Conclusions

Experiments were carried out to investigate the instantaneous velocity field of debris flow based on the PIV measurement technique. The velocity distribution through the flow depth was analyzed based on the experimental results. In addition, a modified model was proposed based on the existing theoretical model for the velocity distribution of sediment-laden flows. Conclusions were as follows:

- (1) Fluid with high viscosity hindered the fast settling of the sediment particles and kept the particles moving a longer distance along flume before falling back to bottom. So the particle distribution was more uniform in debris flows than that in sediment-laden flow.
- (2) Although the velocity magnitude for each flume slope angle was different, the dimensionless debris flow velocity followed the similar trend through the flow depth. With increasing debris flow depth, the debris flow velocity increased when dimensionless flow depth ranged from 0 to 0.7. Better relationship between the dimensionless velocity and the dimensionless flow depth was found with the finer particles. It indicated that compared with the flume slope, the size of the particles had greater effects on dynamic characteristics of debris flows.
- (3) Based on the log-law model for the velocity distribution of sediment-laden flow, a modified item was added to describe vertical velocity distribution. It was found that the calculated results were in good agreement with the experimental ones. The coefficient and index for the modified item was about 0.92 and  $-1/6$ , respectively.

#### Notation

The following symbols are used in this paper:

- $A_1$  The modification coefficient (–)
- $B$  The index of the dimensionless flow depth (m)

$B_f$	The integration constant (-)
$D$	The particle diameter (mm)
$Fr$	Froude number (-)
$g$	The acceleration of gravity ( $m/s^2$ )
$k$	The von Karman constant, $k = 0.4$ (-)
$K_s$	The hydraulic roughness (mm)
$M$	Volume of the mixed viscous liquid (kg)
$R$	The hydraulic radius (m)
$\Delta t$	The time interval (s)
$u$	The mean velocity at the cross-section (m/s)
$u_{max}$	The maximum velocity (m/s)
$u_*$	The friction velocity (m/s)
$v_x$	The particle velocity in the x direction (m/s)
$\bar{v}_x$	The mean velocity in the x direction (m/s)
$v_y$	The particle velocity in the y direction (m/s)
$\bar{v}_y$	The mean velocity in the y direction (m/s)
$\Delta x$	The displacement in the x direction at time interval $\Delta t$ (m)
$y$	The vertical distance from the flume bed (m)
$\Delta y$	The displacement in the y direction at time interval $\Delta t$ (m)

## Greek letters

$\alpha$  Slope angle ( $^\circ$ )


## Disclosure statement


No potential conflict of interest was reported by the authors.

## Funding


The research work was supported by Key International Cooperation Project of the National Natural Science Foundation of China [grant number 41520104002]; Key Research Program of Frontier Sciences, CAS [grant number QYZDY-SSW-DQC006]; and Foundation of Youth Innovation Promotion Association, Chinese Academy of Sciences [grant number 2017425].

## ORCID

Huayong Chen  <http://orcid.org/0000-0003-4033-3339>

Kaiheng Hu  <http://orcid.org/0000-0001-8114-5743>

Peng Cui  <http://orcid.org/0000-0003-2663-301X>

Xiaoqing Chen  <http://orcid.org/0000-0002-0177-0811>

## References

- Arattano M. 2003. Monitoring the presence of the debris-flow front and its velocity through ground vibration detectors. In: Rickenmann D, Chen C-L, editors. Debris flow hazard mitigation: mechanics, prediction and assesment. Rotterdam: Millpress.
- Arattano M, Marchi L. 2005. Measurements of debris flow velocity through cross-correlation of instrumentation data. *Nat Hazards Earth Syst Sci.* 5:137–142.
- Armanini A, Fraccarollo L, Rosatti G. 2009. Two-dimensional simulation of debris flows in erodible channels. *Comput Geosci.* 35(5):993–1006.
- Balachandrar R, Patel VC. 2005. Velocity measurements in a developed open channel flow in the presence of an upstream perturbation. *J Hydraul Res.* 43:258–266.
- Cui P, Zhou Gordon GD, Zhu X, Zhang J. 2013. Scale amplification of natural debris flows caused by cascading landslide dam failures. *Geomorphology.* 182:173–189.

- Di Cristo C. **2011**. Particle imaging velocimetry and its applications in hydraulics: a state-of-the-art review//experimental methods in hydraulic research. Berlin: Springer; p. 49–66.
- Fei X, Cui P, Li Y. **2002**. Concentration and velocity of debris flows. *Int J Sediment Res.* 17:233–243.
- Gabriele A, Tsoligkas AN, Kings IN. **2011**. Use of PIV to measure turbulence modulation in a high throughput stirred vessel with the addition of high Stokes number particles for both up-and down-pumping configurations. *Chem Eng Sci.* 66:5862–5874.
- Guo JK, Julien PY. **2001**. Turbulent velocity profiles in sediment-laden flows. *J Hydraul Res.* 39:11–23.
- Han Z, Chen G, Li Y. **2014**. A new approach for analyzing the velocity distribution of debris flows at typical cross-sections. *Nat Hazards.* 74:2053–2070.
- Han Z, Chen GQ, Li Y, Wang W, Zhang H. **2015**. Exploring the velocity distribution of debris flows: an iteration algorithm based approach for complex cross-sections. *Geomorphology.* 241:72–82.
- Han Z, Li Y, Huang J, Chen GQ, Xu LR, Tang C, Zhang H, Shang YH. **2016**. Numerical simulation for run-out extent of debris flows using an improved cellular automaton model. *Bull Eng Geol Environ.* 1–14. DOI:10.1007/s10064-016-0902-6
- Hungr O, McDougall S. **2009**. Two numerical models for landslide dynamic analysis. *Comput Geosci.* 35:978–992.
- Hürlimann M, Rickenmann D, Graf C. **2003**. Field and monitoring data of debris flow events in the Swiss Alps. *Can Geotech J.* 40:161–175.
- Iverson RM. **2012**. Elementary theory of bed-sediment entrainment by debris flows and avalanches. *J Geophys Res Earth Surf.* 117:3006.
- Jooe DA, Van Steijn H. **2003**. PROMOTOR-df: a GIS-based simulation model for debris-flow hazard prediction. In: Rickenmann D, Chen C-I, editors. Debris-flow hazards mitigation: mechanics, prediction, and assessment. Vols. 1 and 2. Rotterdam: Mill Press.
- Liu P, Lam KM. **2014**. Simultaneous PIV measurements of fluid and particle velocity fields of a sediment-laden buoyant jet. *J Hydro-Environ Res.* 9:314–323.
- Luna BQ, Rémaitre A, Van Asch TWJ, Malet JP, Van Westen CJ. **2012**. Analysis of debris flow behavior with a one dimensional run-out model incorporating entrainment. *Eng Geol.* 128(2):63–75.
- Mangeney A, Tsimring LS, Volfson D, Aranson IS, Bouchut F. **2007**. Avalanche mobility induced by the presence of an erodible bed and associated entrainment. *Geophys Res Lett.* 34:L22401.
- McArdell BW, Zanuttigh B, Lamberti A, Rickenmann D. **2003**. Systematic comparison of debris-flow laws at the Illgraben torrent, Switzerland. In: Rickenmann D, Chen C-L, editors. Debris-flow hazards mitigation: mechanics, prediction, and assessment. Proceedings of the third international conference. Rotterdam: Millpress; p. 647–657.
- Medina V, Bateman A. **2010**. Debris flow entrainment experiments at UPC, interpretation and challenges. In: Martin O, Zhang X, editors. Latest trends on engineering mechanics, structures, engineering geology. Athens: WSEAS Press. p. 38–44.
- Parsons JD, Whipple KX, Simoni A. **2001**. Experimental study of the grain-flow, fluid-mud transition in debris flows. *J Geol.* 109(4):427–447.
- Prochaska AB, Santi PM, Higgins JD. **2008**. A study of methods to estimate debris flow velocity. *Landslides.* 5:431–444.
- Tang C, Rengers N, Van Asch TWJ, Yang YH, Wang GF. **2011**. Triggering conditions and depositional characteristics of a disastrous debris-flow event in Zhouqu city, Gansu Province, northwestern China. *Nat Hazards Earth Syst Sci.* 11:2903–2912.
- Unadkat H, Rielly CD, Hargrave GK. **2009**. Application of fluorescent PIV and digital image analysis to measure turbulence properties of solid–liquid stirred suspensions. *Chem Eng Res Des.* 87:573–586.
- Virdung T, Rasmuson A. **2007**. Solid–liquid flow at dilute concentrations in an axially stirred vessel investigated using particle image velocimetry. *Chem Eng Commun.* 195:18–34.
- Wang X, Wang Z, Yu M, Li D. **2001**. Velocity profile of sediment suspensions and comparison of log-law and wake-law. *J Hydraul Res.* 39:211–217.
- Wang W, Chen G, Han Z, et al. **2016**. 3D numerical simulation of debris-flow motion using SPH method incorporating non-Newtonian fluid behavior. *Nat Hazards.* 81(3):1981–1998.
- Wei F, Yang H, Hu K. **2012**. Measuring internal velocity of debris flows by temporally correlated shear forces. *J Earth Sci.* 23:373–380.
- Wereley ST, Meinhart CD. **2010**. Recent advances in micro-particle image velocimetry. *Annu Rev Fluid Mech.* 42:557–576.
- Yang H, Wei F, Hu K. **2011**. Measuring the internal velocity of debris flows using impact pressure detecting in the flume experiment. *J Mt Sci Engl.* 8:109–116.